Evidence for entropically-controlled interfacial hydration in mesoporous organosilicas

Hyunjin Moon,[†] Ryan P. Collanton,[†] Jacob I. Monroe,[†] Thomas M. Casey,[‡] M. Scott Shell,[†] Songi Han,[†,‡,*] Susannah L. Scott[†,‡,*]

[†]Department of Chemical Engineering, University of California, Santa Barbara, California 93106-5080, United States

[‡]Department of Chemistry & Biochemistry, University of California, Santa Barbara, California 93106-9510, United States

ABSTRACT: At aqueous interfaces, the distribution and dynamics of adsorbates are modulated by the behavior of interfacial water. Hydration of a hydrophobic surface stores entropy via the ordering of interfacial water, which contributes to the Gibbs energy of solute binding. However, there is little experimental evidence for the existence of such entropic reservoirs, and virtually no precedent for their rational design in systems involving extended interfaces. In this study, two series of mesoporous silicas were modified in distinct ways: (1) progressively deeper thermal dehydroxylation, via condensation of surface silanols, and (2) increasing incorporation of non-polar organic linkers into the silica framework. Both approaches result in decreasing average surface polarity, manifested in a blue-shift in the fluorescence of an adsorbed dye. For the inorganic silicas, hydrogen-bonding of water becomes less extensive as the number of surface silanols decreases. Overhauser dynamic nuclear polarization (ODNP) relaxometry indicates enhanced surface water diffusivity, reflecting a loss of enthalpic hydration. In contrast, organosilicas show a monotonic decrease in surface water diffusivity with decreasing polarity, reflecting enhanced hydrophobic hydration. Molecular dynamics simulations predict increased tetrahedrality of interfacial water for the organosilicas, implying increased ordering near the nm-size organic domains (relative to inorganic silicas, which necessarily lack such domains). These findings validate the prediction that hydrophobic hydration at interfaces is controlled by the microscopic length scale of the hydrophobic regions. They further suggest that the hydration thermodynamics of silica surfaces can be tuned to promote adsorption, which can promote selectivity in catalytic reactions.

INTRODUCTION

Interfacial hydration refers to the behavior of water molecules in the vicinity of an interface (typically, at distances ≤ 1 nm). It plays an important role in modulating interfacial dynamics and adsorption energies of solutes. Together, these effects influence the efficiencies of separations and catalysis, which are mediated by the properties of adsorption sites located at both soft and hard liquid interfaces. The mechanisms by which surface hydrophobicity affects solute binding remain poorly understood. For extended surfaces that are flat and chemically uniform, hydrophobicity can be inferred from surface force measurements, in which the repulsive force[1] or equilibrium interaction force[2] between two surfaces correlates with hydrophobicity. Alternately, the receding contact angle (θ) of a water droplet is measured to assess the macroscopic hydrophobicity,[3] defined operationally as θ > 90 °. However, the local hydrophobicity of real surfaces with geometric and chemical heterogeneity, characteristic of many porous materials, is challenging to evaluate. The high curvature (both external and internal) of such surfaces and their fractal nature make them intrinsically ill-suited for conventional macroscopic measurements, which in any case do not provide information at the molecular length scales relevant to adsorption and/or reaction.

Fundamentally, a surface is locally hydrophobic when its Gibbs energy of hydration is positive. However, $\Delta G_{hydration}$ is not readily measured. A more accessible definition of surface hydrophobicity is based on the excess chemical potential, μ_{ex}, of an adsorbed hydrophobic molecule.[4,5] The value of μ_{ex} can be determined from the equilibrium partitioning of the hydrophobe between the surface and the aqueous phase, eq 1,[6,7] where the numerator and denominator of the natural logarithm term represent ratios of the numbers of hydrophobe and water molecules at the surface and in the bulk solution, respectively.

$$\mu^{ex} = -k_B T \ln \left[\frac{n_{hydrophobe}^{surface} / n_{H2O}^{surface}}{n_{hydrophobe}^{total} / n_{H2O}^{total}} \right] \quad (1)$$

Operationally, a surface with a negative value of μ_{ex} is defined as hydrophobic. Although the sign and magnitude of μ_{ex} are not readily measured at the nm scale, μ_{ex} can be computed from molecular dynamics simulations of model hydrophobes, such as methane molecules or Lennard-Jones particles. However, such studies still require a detailed knowledge of the surface structure, which may not be available for real systems. Therefore, experimental methods to evaluate the thermodynamic properties of interfacial water, reflecting the local hydrophobicity of the surface, are needed to verify and benchmark the simulations.

The fluorescence from a solvatochromic dye molecule, such as Prodan, is an indirect probe of hydrophobicity. The emission energy reflects the local polarity,[8,9] which is closely related to hydrophobicity.[10–12] The emission of adsorbed Prodan has been used as an empirical measure of relative average hydrophobicity in a series of mesoporous organosilicas.[13,14] Overhauser Dynamic Nuclear Polarization (ODNP) relaxometry of interfacial water provides another indirect measure of surface hydrophobicity. ODNP relies on cross-relaxation due to dipolar coupling between the ^{1}H nuclear spin of a water molecule and the unpaired electron spin of a nearby radical (*aka* the spin label).

At a magnetic field strength of 0.35 T, this coupling is effective for water molecules whose correlation times for their motion relative to the spin label are in the ps- to sub-ns-range. By immobilizing the spin label at a surface, ODNP becomes sensitive to the translational motion of water molecules near that surface.[15,16] It has been used to assess the diffusivity of water molecules near proteins and other biomolecules labeled with paramagnetic spin probes.[6,17] The diffusivities correlate well with local surface hydrophobicities predicted by computed values of μ_{ex},[6] surface geometric topologies (as measured by local excluded volumes),[6] and solvation entropies.[17]

ODNP relaxometry measurements also provide unique insight into the thermodynamic origins of interfacial hydration. In general, a more hydrophobic surface may have a less negative Gibbs energy of hydration due to (1) a less negative hydration enthalpy (implying weaker binding of water to the surface), and/or (2) a more negative hydration entropy (due to greater ordering of the interfacial water, relative to the bulk).[18–21] Either effect can result in more favorable displacement of surface water by a solute binding to the more hydrophobic surface. However, the dynamics of near-surface water differ in each limiting scenario. When $\Delta G_{hydration}$ is dominated by its enthalpic term, increasing hydrophobicity causes surface water motion to become faster due to the lower enthalpic cost of breaking the hydrogen bonds between water and the surface. The lower cost of dehydration also results in more solute adsorption. In contrast, when the key term in $\Delta G_{hydration}$ is entropic, near-surface water moves more slowly with increasing hydrophobicity. Liberation of the more ordered interfacial water drives solute adsorption.

The cross-over from enthalpically-driven to entropically-driven sorption has been predicted to occur when the hydrophobic domain size decreases below ca. 1 nm.[20–22] Therefore trends in surface water diffusivity can, in principle, reveal information about the length scale of the local hydrophobic domains. Although cross-over has been demonstrated experimentally for highly idealized systems such as individual polymer chains of varying size,[23,24] it has yet to be observed in porous materials with extended surfaces, which are particularly relevant in separations and catalysis.

Amorphous silica is a technologically important material that is widely used as an adsorbent for chemical separations, and as a support for heterogeneous catalysts. In this study, variations in the hydration of amorphous silica were investigated as a function of their surface chemistry. Hydrophobicity was modified in two distinct ways: (1) by increasingly severe thermal treatment, which reduces the silanol/siloxane ratio on the silica surface,[2] and (2) by chemical incorporation of organic linkers having molecular dimensions (ca. 1 nm or less) into the silica framework.[14,25,26] Relative surface polarity was assessed via the fluorescence of adsorbed Prodan. Equilibrium surface water diffusivities were measured using ODNP relaxometry, and combined with molecular dynamics simulations to understand the enthalpic and entropic consequences of solvation for both types of surface modification.

RESULTS

Systematic variation of silica hydrophobicity. Amorphous silicas with hexagonally -ordered mesoporosity (SBA-15-type) were modified to achieve gradually varying surface hydrophobicity. In one series of silica materials, inorganic silica was made by the templated condensation of tetraethylorthosilicate (T) as the sole silica source. This material is named T100 (i.e., 100 mol% T). SEM images show elongated fibers with diameters 0.3-0.6 μm and lengths 2-10 μm (Figure S1). Calcination of T100 at 250 °C removed the templating surfactant. Silanol condensation was achieved at higher temperatures (up to 1000 °C under N_2 flow), resulting in increased surface coverage by non-polar siloxane bonds (Scheme 1a).[27,28] Silicas subjected to this additional thermal treatment are denoted by an appended label indicating the temperature used in partial dehydroxylation. For example, T100-600 refers to inorganic silica treated at 600 °C. Upon heating, the B.E.T. surface area of the silica decreases gradually, from 709 m^2/g for T100 after calcination at 250 °C to 353 m^2/g for T100-1000 after thermal treatment at 1000 °C (Table S1). Thermal treatment eliminates a small contribution from microporosity, but the nanoscale porosity is mostly maintained over this temperature range, as confirmed by small-angle X-ray diffraction (Figure S2). However, the average pore size decreases slightly, from 10 to 7 nm (Table S1 and Figure S3a).

Scheme 1. Illustration of SBA-15-type silica materials used in this study, and their compositional variability: (a) mesoporous inorganic silicas, with variable surface silanol content achieved via thermal treatment, and (b) mesoporous organosilicas, with variable framework linker compositions.

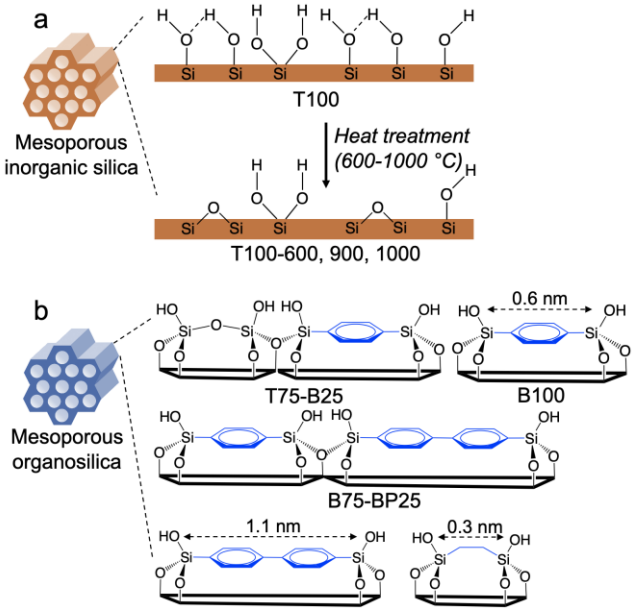

In a second series of silica materials, one or more organodisilanes (containing phenylene, biphenylene, or ethylene linkers) were incorporated into the framework of the ordered mesoporous silica during synthesis (Scheme 1b). Each type organosilica is named according to the organodisilane precursor used (B: 1,4-bis(triethoxysilyl)benzene, BP: 4,4′-bis(triethoxysilyl)1-1′-biphenyl, E: 1,2- bis(trimethoxysilyl)ethane), and its molar proportion. For example, T75-B25 was synthesized by co-condensation of T (75 mol%) and B (25 mol%). In a recent study,[14] we showed that the fraction of phenylene and/or biphenylene linkers in the SBA-15 framework increases gradually without significantly altering the textural properties of the mesoporous silica, such as the B.E.T. surface area (ca. 700 m^2/g) and the pore size (5-10 nm), Table S1 and Figure S3b. However, BP100 has

a broader pore size distribution, compared to other organosilicas.[14]

Table 1. Effect of thermal treatment and framework linkers on surface polarity and near-surface water dynamics in amorphous silicas

Silica [a]	Framework linker(s)				Pore size	Thermal treatment	Silanol density [b]	Prodan emission [c]	Relative polarity [d]	$D_{surface}$
	oxo	phenylene	biphenylene	ethylene	(nm)	(°C)	α_{OH} (nm^{-2})	λ_{max} (nm)		(10^{-10} m^2/s)
T100	•				9.7	-	1.8	508	0.80	10.0 ± 0.2
T100-600	•				8.8	600	1.2	504	0.76	9.4 ± 0.3
T100-900	•				7.9	900	0.9	499	0.71	12.6 ± 0.3
T100-1000	•				7.0	1000	0.5	493	0.66	13.7 ± 0.5
T75-B25	•	•			7.6	-	1.5	500	0.72	7.4 ± 0.2
B100	•	•			7.6	-	1.3	491	0.65	4.3 ± 0.5
B75-BP25	•	•	•		6.3	-	1.8	481	0.56	3.3 ± 0.2
E100	•			•	7.1	-	2.2	479	0.55	4.5 ± 0.5
BP100	•		•		5.0	-	1.6	475	0.52	2.4 ± 0.2
B100-350	•	•			6.0	400	1.0	483	0.58	8.6 ± 0.1

[a] All materials are ordered mesoporous silicas (SBA-15-type), made by condensing silanes in the presence of P123 as templating surfactant. Each material is named according to the type of silane precursor(s) used in its synthesis (T: tetraethylorthosilicate, B: 1,4-bis(triethoxysilyl)benzene, BP: 4,4′-bis(triethoxysilyl)1-1′-biphenyl, E: 1,2-bis(trimethoxysilyl)ethane), and their relative molar proportions. Each material was calcined at 250 °C to remove the templating surfactant, except for E100 (whose lower thermal stability required surfactant removal by extraction in refluxing ethanol). The appended number indicates the temperature (in °C) of subsequent thermal treatment, if any. [b] Silanol content was measured by $VOCl_3$ chemisorption, after evacuation at 170 °C and 0.1 mTorr for 7 h to remove adsorbed water.[14,29] For silicas thermally treated after calcination, the silanol density was measured after immersion in water at room temperature for 3 d, resulting in partial rehydroxylation. The partially rehydroxylated silicas were also dehydrated at 170 °C for 7 h prior to measuring their silanol densities. Surface areas were obtained using the Brunauer-Emmett-Teller (B.E.T.) method, assuming the area occupied by an adsorbed N_2 molecule is 0.135 nm^2 (appropriate for perpendicular adsorption on oxide surfaces).[30] The generally accepted measurement error in B.E.T. surface areas, ± 10 %,[31] leads to an error in the silanol density of ca. 10 %. [c] Measurement error ±1 nm. [d] Relative polarity was interpolated using a calibration curve[32] based on the emission of Prodan in solvents of varying relative polarity (Table S3, Figure S5).[33] The scale is anchored by assigning relative polarity values of 0 and 1 to tetramethylmethylsilane and water, respectively.

The surface silanol density of each silica was quantified by its stoichiometric reaction with $VOCl_3$ vapor.[29] This method gives lower values than H/D exchange methods[34] or analysis by quantitative ^{1}H MAS NMR,[35] however, the latter two methods also count sub-surface silanols that are inaccessible to $VOCl_3$. For example, the density of $VOCl_3$-accessible silanols on T100 calcined at 250 °C is 1.8 nm^{-2} (Table 1), compared to ca. 5 nm^{-2} reported for various silica materials by H/D exchange.[34] The density of $VOCl_3$-accessible silanols decreases gradually with increasing severity of thermal treatment, eventually reaching 0.1 nm^{-2} for T100-1000 (Table S2).

Since the assessment of surface water dynamics by ODNP requires extended exposure of each silica to water, silanol densities were remeasured after immersing each thermally treated T100 silica in water at room temperature for 3 d. (It was not deemed necessary to rehydrate T100, because calcination at 250 °C results in only a small decrease (< 10 %) in its silanol content.)[36] Table S2 shows the changes (typically, 2-5× increases) in silanol density for the water-exposed silicas compared to the dry silicas. This partial rehydroxylation is expected,[37] and limits our ability to make measurements on silicas with very low surface hydroxyl densities. However, the dehydroxylation process is not fully reversed.[38] Therefore the silanol content of the rehydrated T100 silicas still decreases smoothly, from 1.8 to 0.5 nm^{-2} with increasing thermal treatment up to 1000 °C (Table 1).

Organosilicas containing phenylene and biphenylene linkers were not treated thermally, apart from the mild calcination required to remove the templating surfactant. Their silanol densities vary over a smaller range (1.8 - 1.3 nm^{-2}, Table 1), and lack a discernable trend. Ethylene-bridged silica (E100) has a slightly higher silanol density (2.2 nm^{-2}), due to the use of ethanol extraction rather than calcination to remove the templating surfactant (necessitated by the limited thermal stability of E100).[39] Consequently, changes in surface hydrophobicity for the mesoporous organosilicas (with the possible exception of E100) are expected to be associated mainly with the nature and abundance of the organic linkers, rather than variations in their surface silanol content.

Relative polarities of silica surfaces. Changes in surface polarity for the T100 series of thermally treated silicas were assessed by adsorbing Prodan from aqueous solution. To mimic the conditions required for subsequent ODNP measurement of surface water dynamics (see below), each thermally-treated silica was first immersed in water for 3 d, then Prodan was adsorbed from aqueous solution. Fluorescence spectra for the series of inorganic silica powders (dried at 85 °C) are compared

in Figure 1a. The λ_{max} values decrease monotonically from 508 to 493 nm as the thermal treatment increases. Thus, λ_{max} is correlated with silanol density (Table 1, Figure S4).

Fluorescence spectra for the organosilica series with adsorbed Prodan are compared in Figure 1b. The λ_{max} values decrease monotonically as the fraction and size of the organic linkers incorporated into the framework increases. Notably, the presence of these organic linkers has a larger effect on surface polarity than silanol density, as evidenced by the much more significant blueshift (33 nm) of

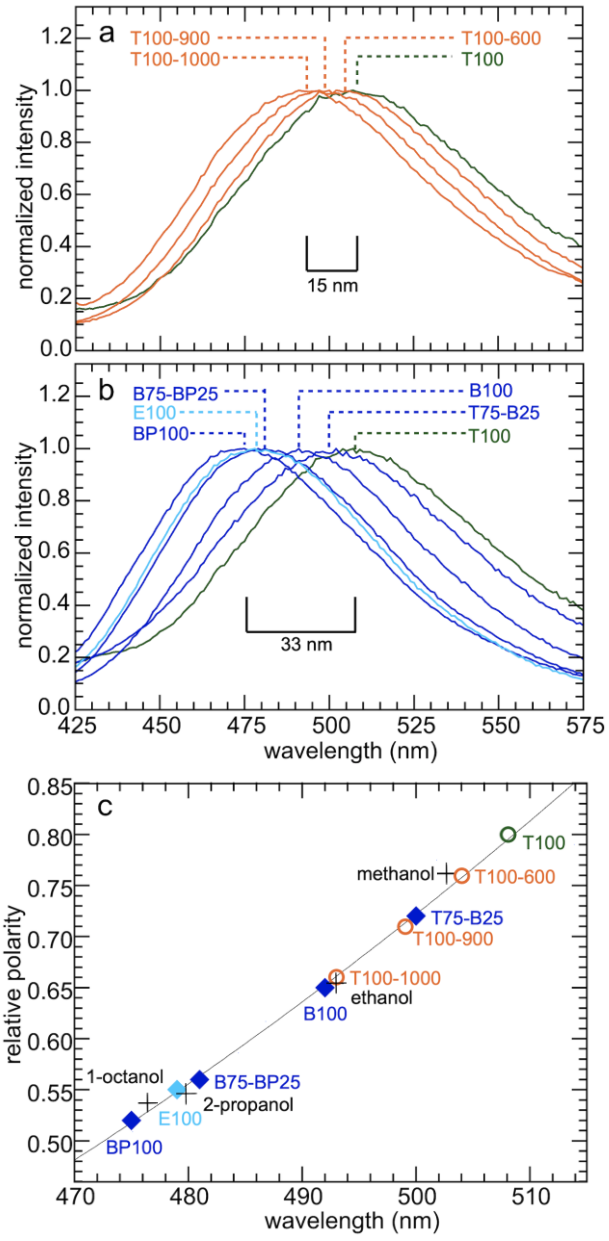

Figure 1. Comparison of fluorescence spectra for Prodan adsorbed on T100 with (a) mesoporous inorganic silicas (T100) after various thermal treatments (indicated by the appended numbers), and (b) various mesoporous organosilicas (not thermally treated, except as necessary for surfactant removal). In each case, spectra were recorded for dry silica powders. (c) Correlation between Prodan fluorescence emission maximum and relative surface polarity, for all mesoporous silicas (T100: green circle; thermally treated inorganic silicas: orange circles; organosilicas: blue diamonds). Several solvent values are also shown for comparison (+).

λ_{max} across the range of organosilicas, compared to just 15 nm for T100 after various thermal treatments.

Relative surface polarities were obtained for each type of silica by interpolating values measured for various solvents, ranging from 1.000 for water to 0.444 for dimethylsulfoxide (Table S3, Figure S5).[32,33] The results are shown in Figure 1c. The relative surface polarities of the inorganic silicas range from 0.80 to 0.66. T100 without thermal treatment is slightly more polar than methanol. Heating this silica to 1000 °C followed by partial rehydroxylation in water at room temperature results in a relative surface polarity similar to ethanol.

In the organosilica series, the relative polarities vary down to 0.52. The polarities of B100 and E100 are similar to ethanol and 2-propanol, respectively, while the least polar material, BP100, is slightly less polar than 1-octanol. For organosilicas containing mixtures of linkers, such as B75-BP25 and T75-B25, intermediate polarities were obtained (Figure S6a). This effect is similar to gradually increasing the carbon chain length in aliphatic alcohols and ketones (Figure S6b),[33] and implies a homogeneous spatial distribution of the organic linkers, without segregation into organic-rich domains.

Probing the dynamics of interfacial water. The mobility of near-surface water provides insight into the thermodynamics of interfacial hydration. ODNP relaxometry probes water motion that occurs near a spin label, such as a stable nitroxide radical. It relies on measurement of the cross-relaxivity (k_σ), i.e., the enhancement of the relaxation rate of the ^{1}H nuclear spin of water due to dipolar coupling to the unpaired electron spin (e) of the spin label.[15,16] ^{1}H-e cross-relaxation is efficient for water located within 1 nm of the spin label, and moving with a correlation time less than or equal to the inverse electron spin Larmor frequency (9.8 GHz at 0.35 T).[15,16] The magnitude of k_σ is directly proportional to the rate of water diffusion near the spin label.[6] More detailed discussions of the ODNP method can be found in the Materials and Methods section, and in the SI.

Molecules moving near an interface diffuse more slowly due to the geometric effect of the surface,[40,41] as well as any chemical interactions with the surface.[2,42] Since the former is expected to be similar for all mesoporous silicas studied here, major differences in water diffusivity can be attributed to differences in chemical interactions between water and the mesopore walls. By attaching 4-carboxy-TEMPO radicals to the pore walls, we ensure that the resulting cross-relaxivity ($k_{\sigma,surface}$) reports only on the diffusivity of water less than ca. 2 nm from the surface (Scheme 2). Thus, considering the pore sizes (6-10 nm) of silicas, ODNP reflects water dynamics near the surface, while for silicas with smaller pores (< 4 nm), water molecules near the surface and in the center of pore both contribute to the ODNP results. Surface water diffusivities $D_{surface}$ were obtained from the measured $k_{\sigma,surface}$ values (see SI). Although the numerical values of $D_{surface}$ cannot be directly compared to surface water diffusivities measured by other techniques that average over different water populations, or capture different types of motion,[43–45] $D_{surface}$ is correlated with surface water diffusivity.

Effect of surface silanol density on water mobility. Since water interacts via hydrogen-bonding to silanols more strongly

than to siloxanes, surface water diffusivity should vary inversely with the surface silanol density. $D_{surface}$ values obtained for each of the thermally -treated T100 silicas are shown in Table 1, Figure 2, and Figure S7a. As expected, the value of $D_{surface}$ is smaller for T100 without thermal treatment, $(10.0 \pm 0.2) \times 10^{-10}$ m^2/s, than for T100-1000, $(13.7 \pm 0.5) \times 10^{-10}$ m^2/s, although the difference is small.

Hydration of inorganic silica surfaces can therefore be attributed principally to enthalpic stabilization associated with hydrogen bonding. Curiously, the change is not gradual: the surface water diffusivity is unchanged when T100 is treated at 600 °C, but rises abruptly when T100 is treated at 900 °C. These findings suggest a non-uniform distribution of surface silanols and the presence of silanol-free hydrophobic domains (see Discussion below).

Scheme 2. Attachment of a 4-carboxy-TEMPO radical to a silica surface via a propylamine tether provides the spin probe for ODNP relaxometry, which measures water dynamics within ca. 1 nm of the radical, therefore within ca. 2 nm of the interface.

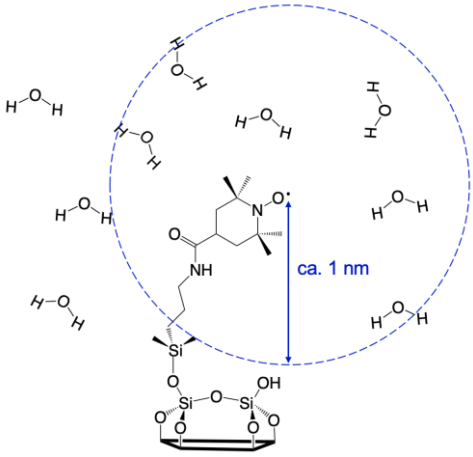

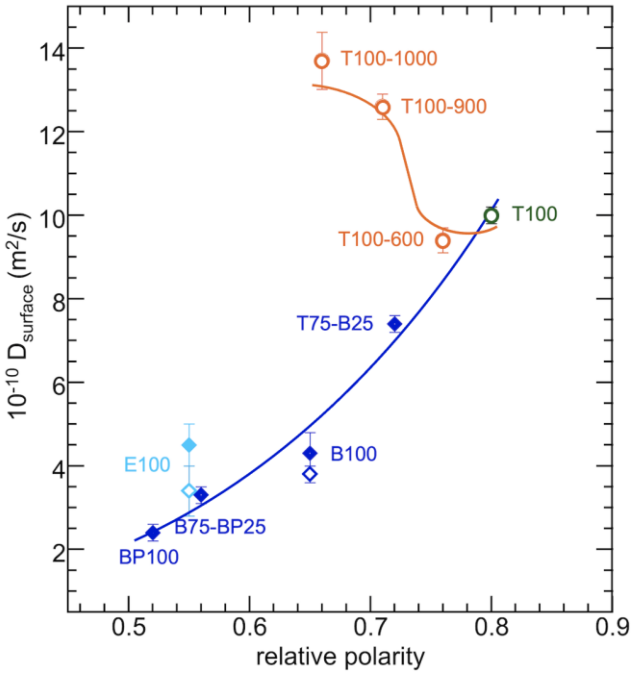

Figure 2. Diffusivity of near-surface water ($D_{surface}$, derived from $k_{\sigma,surface}$ as measured by ODNP relaxometry) in mesoporous silicas containing only oxygen linkers (green and orange circles ○, or a combination of oxygen and organic linkers (blue filled diamonds ◆ for larger pores, ca. 7 nm, and blue hollow diamonds ◇ for smaller pores, ca. 4 nm), as a function of the relative surface polarity (obtained by measuring the fluorescence of adsorbed Prodan, Figure 1c). The solid lines are present only to guide the eye.

Effect of organic linkers on water diffusivity. The behavior of water in the organosilica pores is very different from that of water in the pores of thermally treated inorganic silica. Figure 2 shows the behavior of surface water for the organosilicas as a function of their relative surface polarity (blue diamonds). In contrast to the *inverse* correlation of surface water diffusivity with polarity for the inorganic silicas, $D_{surface}$ is *positively* correlated with surface polarity for the organosilicas. For example, the value of $D_{surface}$ for T100 is twice that for B100, $(4.3 \pm 0.5) \times 10^{-10}$ m^2/s, which in turn is twice that for BP100, $(2.4 \pm 0.2) \times 10^{-10}$ m^2/s. Reducing the pore size of the organosilicas from ca. 7 nm to ca. 4 nm (Figure S8) results in minor changes in surface water diffusivity (Figure 2), suggesting that mesopore confinement effects are minor. Since the silanol density varies little among the organosilicas and shows no obvious influence of $D_{surface}$ (Figure S7b), and since water molecules interact weakly with the organic linkers, the variability in water dynamics near the organosilica surfaces must arise due to differences in entropic rather than enthalpic contributions (see below).

For the ethylene-bridged organosilica E100, the $D_{surface}$ value is higher than expected based on the polarity of this organosilica. It is unlikely that the slightly higher silanol density of E100 is responsible, since $D_{surface}$ is independent of silanol density for organosilicas containing aromatic linkers (Figure S7b). Instead, the smaller ethylene linkers may be less effective than the larger aromatic linkers in inducing low entropy surface hydration.

Partial dehydroxylation of organosilica. The much slower diffusion of interfacial water in the organosilicas relative to the inorganic silicas suggests that water molecules at the water-silica interface become more ordered as surface hydrophobicity increases, resulting in a loss of entropy. Ordering may arise when water molecules form a hydrogen-bonded bridge or dome over the organic moieties, anchored at adjacent silanols (Scheme 3a).

Scheme 3. Ordering of water molecules near organosilica surfaces: (a) chain of hydrogen-bonded water anchored at both edges of an organic linker (the blue dotted lines represent hydrogen bonds); and (b) reduction in ordering upon partial dehydroxylation of the organosilica. The red dotted oval highlights the loss of a hydrogen bond anchoring the water chain via a surface silanol.

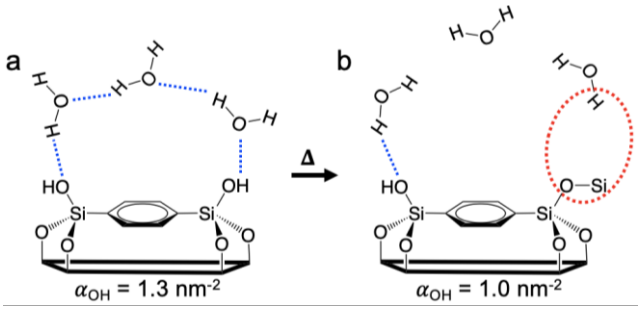

If some of these silanols are removed by thermal condensation, the mobility of the near-surface water should increase due to the resulting decrease in water ordering (illustrated by the dotted red oval in Scheme 3b). To test this hypothesis, B100 was treated thermally at 350 °C, resulting in a 30 % reduction its surface silanol density (from 1.3 to 1.0 nm^{-2}, Table 1). The Prodan fluorescence showed the expected blue-shift from 491 to 483 nm (Figure S9). However, despite its lower polarity (similar to those of B75-BP25 and E100), the surface water diffusivity of B100-350 is double that of B100 prior to its thermal treatment (Table 1). Thus, these measurements depart significantly from the trend of decreasing water diffusivity with increasing polarity observed for the organosilica series, reverting instead to the "normal" behavior of inorganic silica (i.e., water diffusivity *increasing* with decreasing polarity). Apparently, some silanols are key to the effect of the organic linkers on water ordering.

Simulations of water dynamics near silica surfaces. The experimental evidence described above suggests that slower water diffusion near organosilica surfaces, relative to inorganic silica surfaces, arises from increased ordering of water molecules in the hydration layer. To test this hypothesis, molecular dynamics simulations of water near a hydroxylated amorphous silica slab were conducted, in the presence and absence of adsorbed benzene molecules (Figure 3). The cut-offs for defining the hydration layer were chosen to include approximately two hydration layers, based on the density profiles in Figure S10. The surface density of silanol groups was adjusted to 1.5 nm^{-2}, similar to the experimental values. Benzene molecules were placed on the surface to avoid blocking water-silanol interactions, and spaced approximately 1 nm apart. This distance is slightly longer than the expected spacing between phenylene groups of B100 (0.5-0.8 nm).[46] The simplified surface obviously differs from the phenylene-bridged organosilica in that benzene is adsorbed rather than being incorporated into the silica framework, and is present only at the surface rather than being distributed throughout the material. Nevertheless, the model should provide qualitative insight into water dynamics near the experimental surface.

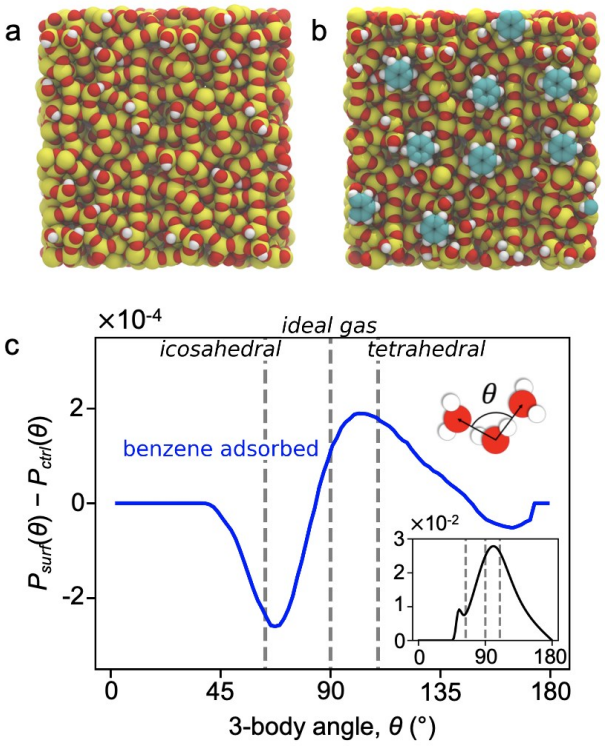

Figure 3. Snapshots of an amorphous silica surface with its silanol density, α_{OH}, adjusted to approx. 1.5 nm^{-2}. Both snapshots were taken after the simulation, such that the surfaces are fully relaxed. Water molecules are removed in order to show the surface structure clearly. (a) The inorganic surface used as a control, and (b) the same surface, with adsorbed benzene molecules. Color scheme: Si, yellow; O, red; C, blue, H, white. (c) Probability distribution of three-body angles (θ) for water near the surface with adsorbed benzene, relative to the distribution for water near the surface without benzene (control). The inset depicts the distribution of three-body angles in the bulk, which is identical for both surfaces.

The benzene-modified surface has a stronger thermodynamic signature of hydrophobicity than the inorganic surface. Specifically, the excess chemical potential μ_{ex}^{HS} for solvating a methane-sized (3.3 Å) hard sphere probe (i.e., an idealized small molecule hydrophobe) near the surface is lower for the adsorbed-benzene surface than for the inorganic surface (Figure S11). Specifically, within 0.8 nm of the surface, the value of μ_{ex}^{HS}/k_BT is (9.390 ± 0.003) for the benzene-modified surface, compared with (10.000 ± 0.004) for the control surface, consistent with increased hydrophobicity for the benzene-modified surface.

Water dynamics were assessed by computing the 2D diffusivity of water in the hydration layer for both silica surfaces. For the surface with adsorbed benzene, the average 2D diffusivity in its hydration layer is (16.5 ± 0.5) × 10^{-10} m^2 s^{-1}, com-

pared to $(20.0 \pm 0.4) \times 10^{-10}$ m^2 s^{-1} for the control surface without benzene. This finding is consistent with the experimental observation of slower water dynamics near organosilica surfaces.

Water structure and its ordering in the hydration layers of both silica surfaces were compared via their three-body angle distributions. These distributions describe the angles subtended by a central water molecule and any two of its nearest neighbors. Compared to a simple fluid without directional interactions (e.g., liquid argon), the three-body angle distribution for water shows a pronounced shift in population towards the tetrahedral angle (i.e., showing stronger preference for angles of ca. 109.5 °).[47,48] In general, the presence of a surface causes the three-body angle distribution of near-surface water molecules to change, relative to the distribution in bulk water.

Previously, a shift towards a reduction in tetrahedral population relative to bulk water was seen in the hydration of flat, extended, hydrophobic surfaces,[47] while an enhanced tetrahedral population relative to bulk water appeared as a signature of nm-scale hydrophobe solvation.[48] In this work, water near the benzene-modified surface shows increased tetrahedral ordering, compared to water near the inorganic surface (Figure 3c). That is, adsorbed benzene induces increased tetrahedrality in the hydration-layer water, shifting the population of near-tetrahedral angles closer to that of bulk water, and hence representing a signature consistent with nm-scale hydrophobe solvation. A decrease in water-water hydrogen bonding (Figure S12) shows that the presence of benzene also reduces the number of hydrogen-bond partners for interfacial water molecules, with those that remain exhibiting increased tetrahedrality. Hence, interfacial waters have fewer equal-energy configurational arrangements (i.e., reduced entropy) that, for pure silica surfaces, enable more facile rearrangement and movement.

DISCUSSION

Tuning hydrophobicity is a powerful method to control solute adsorption. For example, enzymes use hydrophobic hydration to facilitate solute binding to their active sites.[49,50] In these systems, locally ordered interfacial water molecules serve as a low entropy reservoir. Similarly, the liberation of ordered solvent molecules from hydrophobic zeolite micropores leads to large entropy gains upon solute adsorption, compensating for the enthalpic penalties associated with solvent reorganization.[51–53] In heterogeneous catalysis, such entropic effects can influence the overall energetics of adsorption, stabilize transition states, and ultimately increase catalytic activity.[52–54] The enhanced tetrahedrality of water next to moderately hydrophobic pore surfaces has been reported to promote clathrate nucleation for gas storage (e.g., methane, carbon dioxide).[55–57] Designing porous materials with precisely configured hydrophobicity is hampered by the paucity of information about the hydration properties of catalyst surfaces (usually, internal pore surfaces) and the chemical potentials of adsorbed solute molecules. Previous reports on interstitial water dynamics in ordered mesoporous (organo)silicas relied on ^{1}H NMR T_1 and T_2 relaxation times,[43] or Pulsed Field Gradient (PFG) NMR measurements,[58] but neither technique is surface sensitive. Raman spectroscopy with multivariate curve resolution,[21] or THz absorption spectroscopy combined with MD simulations,[59] have been used to describe structural and thermodynamic properties of water in the presence of ordered mesoporous (organo)silicas, but neither technique measures water dynamics near the internal surfaces. Sum Frequency Generation Vibrational Spectroscopy (SFG-VS) has been used to study water structure at flat silica surfaces,[60] but it cannot be applied to the study of water in porous materials. In contrast, ODNP can be used to obtain information on hydration thermodynamics in pores when the internal surfaces are functionalized with a spin probe.

As inorganic mesoporous silica (T100) becomes more hydrophobic due to progressive removal of its surface silanols, the diffusivity of near-surface water increases slightly. This change is consistent with a decrease in the number of hydrogen-bonding interactions between water molecules and surface silanol groups, which results in a reduced enthalpy of surface hydration. Interestingly, the increase in diffusivity shown in Figure 2 is not gradual: there is negligible difference in water diffusivity for surface silanol densities of 1.8 and 1.2 nm^{-2} (corresponding to no additional thermal treatment, and thermal treatment at 600 °C, respectively), followed by an abrupt increase when the surface silanol density declines to 0.9 nm^{-2} (corresponding to thermal treatment at 900 °C). A further decrease in silanol density to 0.5 nm^{-2} (after thermal treatment at 1000 °C) results in negligible further change in diffusivity.

Similar observations were made in a recent study of water mobility near the surface of a non-porous silica, where the discontinuity appeared between pre-treatment temperatures of 700 and 800 °C.[2] It was attributed to disruption of a contiguous 2D water percolation network (consisting of silanol-waters-silanol, connected through hydrogen bonds), which is present only above a threshold silanol density (ca. 1 nm^{-2} for mesoporous inorganic silica, Table 1, Figure S7a). On silicas treated at lower temperatures, silanol clustering requires departures from a random distribution of surface silanols that allow the hydrogen-bond network to persist, even as the total silanol content varies significantly.[2,61–63] This type of clustering implies, by corollary, the presence of large silanol-free regions which interact weakly with water due to the low polarity of siloxane bonds.

In contrast to the modest effect of decreasing silanol density on water mobility, increasing surface hydrophobicity via the incorporation of organic linkers into the silica framework results in a much more dramatic change in the dynamics of interfacial water. Furthermore, the monotonic change is *in the opposite direction*. The presence of organic groups appears to alter water dynamics by a mechanism that is entirely different from a scarcity of silanols, indicating that structural heterogeneity significantly affects the hydration dynamics.[63,64] The slowing of surface water dynamics with increasing surface hydrophobicity in the organosilica series strongly suggests ordering of water molecules around the organic moieties, i.e., the embedded hydrophobic linkers are hydrated by low entropy water. Thus, our results demonstrate the connections between interfacial water structure (e.g., tetrahedrality), thermodynamics (e.g., density profiles, methane chemical potential), and dynamics (e.g., diffusivity) of water hydrating the surfaces of organosilicas.

The computed structural shift towards increased tetrahedrality of interfacial water near the benzene-modified surface is consistent with hydrophobic regions hydrated by ordered water. The established theoretical framework for the hydration of hydrophobic molecules predicts increased ordering of interfacial water and a corresponding reduction in entropy. However, our findings contrast with previous simulations of water behavior

near extended hydrophobic surfaces, which show that diffusivity increases as the hard-sphere chemical potential decreases (i.e., as the surface becomes thermodynamically more hydrophobic).[4] Nevertheless, a study of the temperature dependence of the interfacial tension between aliphatic hydrocarbons and water revealed that the sign of $\Delta S_{hydration}$ changes from negative to positive as the hydrocarbon chain length decreases.[18] Thus, the hydration of very small hydrophobes is entropy-driven. Since interfacial water molecules appear to experience the organic linkers in organosilica frameworks as discrete, small-scale perturbations to the extended silica surface, the hydration of these surfaces should also be entropy-driven.

A quantitative theoretical framework exists to estimate the hydrophobic length-scale for entropic-enthalpic reversal in the Gibbs energy of hydration. Lum-Chandler-Weeks theory predicts that $\Delta G_{hydration}$ is dominated by entropy and scales with volume for small hydrophobes, while for larger hydrophobes $\Delta G_{hydration}$ is dominated by enthalpy and scales with the exposed surface area,[22] since the hydration dynamics are governed by interface formation. The transition is expected to occur on the nm length-scale. Studies of model hydrophobes also predict a characteristic length of ca. 1 nm for entropic-enthalpic reversal.[19,20,22,65,66] Experimentally, water ordering has been observed for small hydrophobic solutes such as alkanes, alcohols and single polymer chains whose length-scales are, indeed, ≤ 1 nm.[21,24,67,68] Such small solutes are encaged by laterally hydrogen-bonded water (i.e., not directly interacting with the hydrophobe), without disrupting the hydrogen-bond network of the surrounding water medium.

In principle, entropic-enthalpic reversal may also occur in materials with extended surfaces (i.e., with dimensions much larger than nm) provided the chemical features themselves have nm-scale dimensions. However, such observations have not previously been made. Assuming the hydrophobic domains on organosilica surfaces are uniformly distributed, the domain length scale is determined mainly by the Si-Si distance associated with the Si-R-Si linker. Using typical Si-C and C-C bond lengths,[69–71] the relevant Si-Si distances are estimated to be 0.3, 0.6, and 1.1 nm for E100, B100, and BP100, respectively (Scheme 1). These sizes are comparable to the predicted crossover length scale (ca. 1 nm) for entropically- vs. enthalpically-driven hydration.[20,22,72] The low entropy reservoirs are proposed to consist of several water molecules that form a hydrogen-bonded bridge (or dome) over the organic domains, anchored by silanols located at the periphery (Scheme 3). Increasing the density of surface organic groups generates more low entropy "hotspots", leading to gradually decreasing surface water mobility.

This picture is consistent with a 2D ^{1}H-^{13}C heteronuclear correlation (HETCOR) NMR study of ordered mesoporous organosilicas that suggested water molecules are not present near hydrophobic framework organic linkers, but occupy the near-surface region and form hydrogen bonds with the hydrophilic inorganic regions.[58] This picture contrasts with a previous report which suggested that benzene interacts with water via π-hydrogen bonding, based on a red-shift for the O-H stretch observed by Raman.[73] However, our modeling studies found no evidence for such interactions. Our observation of decreased water mobility on organosilica surfaces is also consistent with a quasi-elastic neutron scattering (QENS) study which reported an elevated population of slow-moving surface water in a mesoporous organosilica with biphenylene linkers.[74] The authors proposed that alternating hydrophilic silanol and hydrophobic biphenylene groups inhibit the surface diffusion of water.[74] Since removal of the anchoring silanols should lead to an increase in surface water diffusivity, we predicted that thermal treatment of B100 at 350 °C, which induces partial dehydroxylation, should result in a higher $D_{surface}$ value. Our experimental results confirm that the silanol groups adjacent to the organic linkers contribute to the formation of ordered interfacial water.

CONCLUSIONS

The thermodynamic properties of interfacial water are key in modulating the strength of solute binding to surfaces in aqueous environments. The mechanism by which the surface chemistry affects the local thermodynamic properties of interfacial water on real surfaces has been poorly understood, thus the deliberate design of inorganic surfaces in order to control surface water dynamics is still in its infancy.

In this study, the effects of two types of progressive surface modification were investigated to make amorphous silica gradually more hydrophobic: (1) decreasing the silanol/siloxane ratio by thermal treatment, thereby creating large patches of hydrophobic, silanol-free regions that interact weakly with water, and (2) incorporating organic linkers into the silica framework, resulting in small hydrophobic domains that induce local ordering of interfacial water (hydrophobic hydration). Consequently, the enthalpic and entropic contributions to surface hydration were separately and deliberately altered by modulating the surface chemistry of silica.

The ability to design low entropy "hotspots" with locally ordered water in silica mesopores presents new opportunities for tuning the strength of solute adsorption, promoting the formation of clathrates, and enabling improvements in the efficiency of separations and catalysis in porous materials.

EXPERIMENTAL AND COMPUTATIONAL METHODS

Chemicals. Tetraethylorthosilicate (T, 98%), 1,4-bis(triethoxysilyl)benzene (B, 96%), 4,4′-bis(triethoxysilyl)1-1′-biphenyl (BP, 95%), 1,2-bis(trimethoxysilyl)ethane (E, 96%), Pluronic 123, Brij®S10, vanadium oxytrichloride (99%), ammonium metavanadate, hydrogen peroxide (30 wt% in H_2O), sulfuric acid (95.0 - 98.0 wt%), hydrochloric acid (37 wt%), *N*-(3-dimethylaminopropyl)-*N*-ethylcarbodiimide hydrochloride, 2-(*N*-morpholino)ethanesulfonic acid (MES), and *N*,*N*-dimethyl-6-propionyl-2-naphthylamine (Prodan), were purchased from Sigma Aldrich. 4-Carboxy-TEMPO and 3-aminopropyldimethylethoxysilane were purchased from Santa Cruz Biotechnology and Gelest, Inc., respectively. All were used as-received.

Syntheses and thermal pretreatments of mesoporous silicas. Silicas (pore sizes: 5-10 nm) were synthesized followed a previously described procedure,[14] with the exception of E100. The reagent amounts used to obtain each material are shown in Table S4. E100 was synthesized by modifying previously reported methods.[75,76] P123 (3.0 g) was dissolved in aqueous HCl (106 mL, 0.2 M) by stirring at 150 rpm overnight in a Pyrex glass flask at room temperature. 1,2-Bis(trimethoxysilyl)ethane (16 mmol) was injected dropwise. The mixture was heated to 40 °C in a warm water bath and agitated for 23 h. The

reaction mixture was removed from the water bath and transferred to a Parr pressure vessel equipped with a Teflon liner (125 mL). The reactor was sealed and placed in an oven at 100 °C for 48 h. After cooling to room temperature, the resulting suspension was filtered and washed with ~500 mL water, then mixed with ~200 mL ethanol and stirred at 60 °C overnight. After filtering to remove ethanol containing the P123 surfactant, the surfactant extraction was repeated twice more.

B100 and E100 with smaller pore sizes (ca. 4 nm) were synthesized modifying a previously reported procedure.[77] For the synthesis of small-pore B100, Brij®S10 (2.3 g) was dissolved in aqueous HCl (106 mL, 0.8 M) at 50 °C by stirring at 150 rpm for 1 h. 1,4-Bis(triethoxysilyl)benzene (15 mmol) was added, and the mixture was stirred at 50 °C for a further 20 h. After transferring the mixture to a Parr pressure vessel, the reactor was placed in an oven at 100 °C for 48 h. After cooling to room temperature, the solid was washed with water, then suspended in ethanol (200 mL) and stirred overnight at 60 °C. After filtration, residual surfactant was removed by calcination in air at 250 °C for 3 h (ramp rate: 3 °C/min). The same procedure was used to synthesize small-pore E100, except for the surfactant removal step. The ethanol extraction was performed as described above three times at 60 °C, and the calcination step was omitted.

Partially dehydroxylated inorganic silicas were obtained by heating T100 (500 mg) to the desired temperature in a tube furnace at a ramp rate of 10 °C/min in a flow of dry N_2, then holding for 6 h. To partially dehydroxylate B100, the organosilica (100 mg) was heated at 350 °C for 3 h in a flow of dry N_2. After thermal treatment, silicas were stored in air prior to use. Readsorption of moisture from the laboratory ambient therefore partially restored their hydroxyl content. Further rehydroxylation occurred during functionalization with 4-carboxy-TEMPO via propylamine linkers attached to the surface silanol groups, following a previously described method.[14]

Characterization of silica morphology. SEM images were obtained using a ThermoFisher Apero C LoVac Field Emission Gun Scanning Electron Microscopy (FEG SEM). X-ray powder diffraction patterns of air-exposed silicas were acquired using a Rigaku X-ray diffractometer equipped with Cu Kα radiation. N_2 sorption isotherms were measured at 77 K using a 3Flex Surface Characterization Analyzer (Micrometrics). Before each measurement, the silica was heated at 150 °C for 8 h in flowing N_2 to remove adsorbed water. Apparent surface areas were measured using the Brunauer-Emmett-Teller (B.E.T.) method, assuming a molecular area for adsorbed N_2 of 0.135 nm^2.[30] Pore size distributions were obtained by analyzing the adsorption branches of the isotherms, using the Barrett-Joyner-Halenda (B.J.H.) method.

Surface hydroxyl density measurements. Physically adsorbed water was removed from each silica by evacuation in a Schlenk tube at 170 °C and 10^{-4} Torr for 7 h. A portion of the dry silica (30 mg) was exposed to excess $VOCl_3$ vapor for 25 min to convert accessible silanols (≡SiOH) to ≡$SiOVOCl_2$, according to a previously described procedure.[29] The chemisorbed vanadium was extracted from a precisely weighed sample in air (approx. 10 mg) with a freshly-made H_2SO_4 solution (1 M, 5.0 mL) containing H_2O_2 (0.26 M). The UV-vis spectrum of the resulting solution was measured using a UV-2401 spectrophotometer (Shimadzu). The absorbance at 448 nm was converted to vanadium loading using a calibration curve prepared using ammonium metavanadate.

Assessment of surface polarity. Each silica (20 mg) was immersed in water (1 mL) for 3 d, then an aqueous solution of Prodan (5 mL, 30 μM) was added, and stirred for 1 h. The mixture was centrifuged at 3000 rpm for 3 min, then the supernatant liquid was decanted. The wet solid containing adsorbed Prodan was dried using a rotary evaporator (Buchi Rotavapor R-210) at 30 °C and 100 mbar. After removing liquid water, the silica was further dried at 85 °C for 2 h in the oven and fluorescence spectrum was measured with a FluoroMax 4 fluorimeter (Horiba), using an excitation wavelength of 365 nm. The peak maximum λ_{max} was obtained from the zero-crossing of the first-derivative. In order to estimate the relative polarity of silica surfaces, λ_{max} values for Prodan dissolved in various solvents[32] were correlated with reported values for relative solvent polarity.[33] A second-order polynomial function fitted to the data was used to interpolate relative polarities for silicas based on their λ_{max} values.

Overhauser dynamic nuclear polarization (ODNP) NMR relaxometry. Functionalization of silica by 4-carboxy-TEMPO followed a previously described procedure.[14] Spin concentrations (typically, 3-10 μmol/g) were estimated by comparison of the double integral of the EPR spectrum to the value for an aqueous solution of 4-carboxy-TEMPO (0.200 mM). A sample of spin-labeled silica suspended in water (40-80 mg/mL) was loaded into a quartz capillary tube (0.60 mm I.D., 0.84 mm O.D). The X-band continuous-wave (CW) EPR spectrum was recorded using a Bruker EMX CW EPR spectrometer equipped with a Bruker ER-4119HS-LC resonator, operating at a microwave frequency of ca. 9.3 GHz, 1 mW microwave power, 100 kHz modulation frequency, and 0.4 G modulation amplitude.

ODNP measurements were conducted at room temperature using a Bruker EMX CW EPR spectrometer and a Bruker Avance III NMR console. The sample was positioned inside the coil of a home-built NMR probe. The coil, an oval-shaped Helmholtz pair, was tuned and matched using an RLC circuit consisting of two variable capacitors and one fixed inductor. The coil and sample were positioned in the center of a microwave cavity (ER 4119HS-LC, Bruker Biospin). The software Xenon was used to tune the cavity. An EPR spectrum was acquired to identify the magnetic field value at the center of the spectrum (ca. 348.5 mT) and the resonant frequency of the loaded cavity (ca. 9.78 GHz). The NMR probe was subsequently tuned to the ^1H Larmor frequency at the magnetic field used in the experiments (ca. 14.83 MHz). NMR signal enhancements were measured upon irradiation of the central EPR resonance of the nitroxide radical, using applied microwave powers up to a maximum of approx. 6 W. The data used to calculate hydration parameters consist of an array of NMR signal enhancements measured as a function of applied microwave power, and the corresponding array of ^1H longitudinal relaxation times (T_1) at each applied microwave power.

Hydration parameters were calculated following previously published procedures.[16,78–80] The NMR signal enhancement with microwave power caused by the Overhauser effect is asymptotic, due to the saturation behavior of the electron spin transition. An equation modeling the saturation profile was fitted to the data describing the enhancement profile. The "cross-relaxivity", k_σ, accounts for the effective rate of hyperpolarization, which is directly related to the rate of diffusion of water molecules near the spin label.[15] A more detailed explanation is presented in the SI.

Computational Methods. MD simulations were performed in GROMACS (release 2016.1)[81] using the TIP4P-Ew water model,[82] in conjunction with force field parameters developed for models of amorphous silica interfaces.[83] The model used here is approximately 4 nm × 4 nm, and 2 nm thick. The PARMED package[84] was used to decrease the silanol density to approx. 1.5 OH/nm^2, by identifying pairs of silanols to undergo condensation. A hydroxyl group and a proton were removed before creating a siloxane bond between the remaining oxygen and the undercoordinated silicon. Silanol pairs considered for condensation were those with Si-Si distances ≤ 0.55 nm and O-O distances ≤ 0.45 nm. H-bonded silanol pairs with O-O distances ≤ 0.35 nm and O-H-O angles > 110 ° were removed first, before proceeding to condense other pairs.

To model the organosilica surface, benzene molecules were placed onto the silica surface at locations chosen to avoid covering the silanols. Parameters for benzene were obtained from the Automated Topology Builder.[85,86] An energy minimization was performed in vacuum with surface silicon atoms frozen, to allow the benzene molecules to achieve low-energy, adsorbed configurations. All surfaces were then solvated with 1840 water molecules and subjected to further energy minimization, while keeping surface silicon atoms and adsorbed benzene molecules frozen. After the simulation box dimension perpendicular to the interface was adjusted so that the water density far from the interface (bulk water, at least 1 nm from the silica surface) was close to its pressure-equilibrated value, a final energy minimization was performed with only silicon atoms frozen (in order to preserve the surface structure).

In all simulations, the time-step was 0.002 ps, with coordinates output every 0.5 ps. Equilibration consisted of an initial constant-volume run of 100 ps using a Berendsen thermostat[87] with a coupling constant of 0.5 ps. Subsequently, the system was equilibrated with 200 ps of NPT simulation using the same thermostat and a Berendsen barostat set to 1 bar acting only on the dimension perpendicular to the box, with a coupling constant of 5 ps and a compressibility of 4.5 ×10^{-5} bar^{-1}. The constant pressure simulation was repeated to calculate the average box dimension perpendicular to the interface. The simulation box was scaled accordingly and 100 ps of further equilibration was performed in the NVT ensemble using a Nose-Hoover thermostat[88,89] at 300 K and with a coupling constant of 2 ps. The final production run, for which all analyses were performed, used the same thermostat for a total 10 ns. Dynamics were propagated with the velocity Verlet algorithm,[90] and all bonds involving hydrogen were constrained via LINCS.[91] Throughout all MD simulations, the surface silicon atoms as well as three of the carbon atoms in all benzene rings were position-restrained with spring constants of 1000 kJ/mol·nm, allowing the surface hydroxyl groups to move and form hydrogen bonds freely with water. Lennard-Jones and Coulombic pair interactions were cut and shifted to zero at 1.2 nm, with long-range electrostatics handled by the Smooth Particle Mesh Ewald algorithm using GROMACS default parameters.[92]

Three-body angle distributions were calculated as described in the literature,[48] considering the angle between all pairs of water oxygens within a radial distance of 0.332 nm (approx. the first RDF minimum for TIP4P-Ew water at ambient temperature and pressure) from a central water oxygen. Three-body angle distributions at surfaces consider only water oxygens within 0.8 nm of the mean interface, defined as the distance from the surface where the water oxygen density reaches 9.96 nm^{-3} (i.e., approx. 30 % of the bulk density). The pytraj package[93] was used to analyze the simulation trajectories.

Excess chemical potential of hard-sphere insertion is defined as $\mu_{ex}^{HS} = k_B T \ln p_V$, where p_V is the probability of successful insertion of a hard sphere of volume V, considering all configurations sampled during the simulation trajectory.[4] Successful insertions result when there is no overlap of the hard sphere with the centers of any water oxygen or surface heavy atoms. In this work, p_V was computed as a function of distance from the mean silica-water interface by counting the number of successful insertions of hard spheres of volume V placed at random locations in 2D planes of varying distance z from the surface.

ASSOCIATED CONTENT

Supporting Information

The Supporting Information is available free of charge on the ACS Publications website.

SEM images, XRD patterns, physicochemical properties, silanol densities, surface water diffusivities, relative polarities, Prodan dye emission maxima, simulations of number density of Si, O, and C, excess chemical potential of methane-sized hard-sphere probe, description of the ODNP method (PDF).

AUTHOR INFORMATION

Corresponding Authors

*** Songi Han** − Department of Chemistry & Biochemistry, and Department of Chemical Engineering, University of California, Santa Barbara, California 93106, United States; orcid.org/0000-0001-6489-6246; Email: songihan@ucsb.edu

*** Susannah L. Scott** − Department of Chemistry & Biochemistry, and Department of Chemical Engineering, University of California, Santa Barbara, California 93106, United States; orcid.org/0000-0003-1161-0499; Email: sscott@ucsb.edu

Authors

Hyunjin Moon − Department of Chemical Engineering, University of California, Santa Barbara, California 93106, United States

Ryan P. Collanton − Department of Chemical Engineering, University of California, Santa Barbara, California 93106, United States

Jacob I. Monroe − Department of Chemical Engineering, University of California, Santa Barbara, California 93106, United States

Thomas M. Casey − Department of Chemistry & Biochemistry, University of California, Santa Barbara, California 93106, United States

M. Scott Shell − Department of Chemical Engineering, University of California, Santa Barbara, California 93106, United States

Author Contributions

HM synthesized the materials and made the measurements, with assistance of TMC in the analysis of ODNP measurements. RPC and JIM performed the simulations. The manuscript was written with contributions from all authors. All authors have given approval to the final version of the manuscript.

Notes

The authors declare no competing financial interest.

ACKNOWLEDGMENT

We acknowledge funding from the U.S. National Science Foundation (NSF), Award No. CHE-1800596. Some experiments made use of the MRL Shared Experimental Facilities, supported by the

MRSEC Program of the NSF under Award No. DMR-1720256. Support for the ODNP studies was provided by the Deutsche Forschungsgemeinschaft (DFG, German Research Foundation) under Germany's Excellence Strategy—EXC-2033—Project No. 390677874

REFERENCES

(1) Vigil, G.; Xu, Z.; Steinberg, S.; Israelachvili, J. Interactions of Silica Surfaces. *J. Colloid Interface Sci.* **1994**, *165*, 367–385.
(2) Schrader, A. M.; Monroe, J. I.; Sheil, R.; Dobbs, H. A.; Keller, T. J.; Li, Y.; Jain, S.; Shell, M. S.; Israelachvili, J. N.; Han, S. Surface Chemical Heterogeneity Modulates Silica Surface Hydration. *Proc. Natl. Acad. Sci. U. S. A.* **2018**, 201722263.
(3) Law, K. Y. Definitions for Hydrophilicity, Hydrophobicity, and Superhydrophobicity: Getting the Basics Right. *J. Phys. Chem.* **2014**, *5*, 686–688.
(4) Monroe, J. I.; Shell, M. S. Computational Discovery of Chemically Patterned Surfaces That Effect Unique Hydration Water Dynamics. *Proc. Natl. Acad. Sci. U. S. A.* **2018**, *115*, 8093–8098.
(5) Xi, E.; Venkateshwaran, V.; Li, L.; Rego, N.; Patel, A. J.; Garde, S. Hydrophobicity of Proteins and Nanostructured Solutes Is Governed by Topographical and Chemical Context. *Proc. Natl. Acad. Sci. U. S. A.* **2017**, *114*, 13345–13350.
(6) Barnes, R.; Sun, S.; Fichou, Y.; Dahlquist, F. W.; Heyden, M.; Han, S. Spatially Heterogeneous Surface Water Diffusivity around Structured Protein Surfaces at Equilibrium. *J. Am. Chem. Soc.* **2017**, *139*, 17890–17901.
(7) Acharya, H.; Vembanur, S.; Jamadagni, S. N.; Garde, S. Mapping Hydrophobicity at the Nanoscale: Applications to Heterogeneous Surfaces and Proteins. *Faraday Discuss.* **2010**, *146*, 353.
(8) Baral, S.; Phillips, M.; Yan, H.; Avenso, J.; Gundlach, L.; Baumeier, B.; Lyman, E. Ultrafast Formation of the Charge Transfer State of Prodan Reveals Unique Aspects of the Chromophore Environment. *J. Phys. Chem. B* **2020**, *124*, 2643–2651.
(9) Klymchenko, A. S. Solvatochromic and Fluorogenic Dyes as Environment-Sensitive Probes: Design and Biological Applications. *Acc. Chem. Res.* **2017**, *50*, 366–375.
(10) Giovambattista, N.; Debenedetti, P. G.; Rossky, P. J. Effect of Surface Polarity on Water Contact Angle and Interfacial Hydration Structure. *J. Phys. Chem. B* **2007**, *111*, 9581–9587.
(11) Kanduč, M.; Schlaich, A.; Schneck, E.; Netz, R. R. Water-Mediated Interactions between Hydrophilic and Hydrophobic Surfaces. *Langmuir* **2016**, *32*, 8767–8782.
(12) Hamilton, W. C. A Technique for the Characterization of Hydrophilic Solid Surfaces. *J. Colloid Interface Sci.* **1972**, *40*, 219–222.
(13) Singappuli-Arachchige, D.; Manzano, J. S.; Sherman, L. M.; Slowing, I. I. Polarity Control at Interfaces: Quantifying Pseudo-Solvent Effects in Nano-Confined Systems. *ChemPhysChem* **2016**, *17*, 2982–2986.
(14) Moon, H.; Han, S.; Scott, S. L. Tuning Molecular Adsorption in SBA-15-Type Periodic Mesoporous Organosilicas by Systematic Variation of Their Surface Polarity. *Chem. Sci.* **2020**, *11*, 3702–3712.
(15) Biller, J. R.; Barnes, R.; Han, S. Perspective of Overhauser Dynamic Nuclear Polarization for the Study of Soft Materials. *Curr. Opin. Colloid Interface Sci.* **2018**, *33*, 72–85.
(16) Franck, J. M.; Pavlova, A.; Scott, J. A.; Han, S. Quantitative Cw Overhauser Effect Dynamic Nuclear Polarization for the Analysis of Local Water Dynamics. *Prog. Nucl. Magn. Reson. Spectrosc.* **2013**, *74*, 33–56.
(17) Fisette, O.; Päslack, C.; Barnes, R.; Isas, J. M.; Langen, R.; Heyden, M.; Han, S.; Schäfer, L. V. Hydration Dynamics of a Peripheral Membrane Protein. *J. Am. Chem. Soc.* **2016**, *138*, 11526–11535.
(18) Kauzmann, W. Some Factors in the Interpretation of Protein Denaturation. In *Advances in Protein Chemistry*; Academic Press, 1959; Vol. 14, pp 1–63.
(19) Athawale, M. V.; Jamadagni, S. N.; Garde, S. How Hydrophobic Hydration Responds to Solute Size and Attractions: Theory and Simulations. *J. Chem. Phys.* **2009**, *131*, 115102.
(20) Huang, D. M.; Geissler, P. L.; Chandler, D. Scaling of Hydrophobic Solvation Free Energies. *J. Phys. Chem. B* **2001**, *105*, 6704–6709.
(21) Davis, J. G.; Gierszal, K. P.; Wang, P.; Ben-Amotz, D. Water Structural Transformation at Molecular Hydrophobic Interfaces. *Nature* **2012**, *491*, 582–585.
(22) Lum, K.; Chandler, D.; Weeks, J. D. Hydrophobicity at Small and Large Length Scales. *J. Phys. Chem. B* **1999**, *103*, 4570–4577.
(23) Li, I. T. S.; Walker, G. C. Signature of Hydrophobic Hydration in a Single Polymer. *Proc. Natl. Acad. Sci. U. S. A.* **2011**, *108*, 16527–16532.
(24) Di, W.; Gao, X.; Huang, W.; Sun, Y.; Lei, H.; Liu, Y.; Li, W.; Li, Y.; Wang, X.; Qin, M.; Zhu, Z.; Cao, Y.; Wang, W. Direct Measurement of Length Scale Dependence of the Hydrophobic Free Energy of a Single Collapsed Polymer Nanosphere. *Phys. Rev. Lett.* **2019**, *122*, 047801.
(25) Asefa, T.; MacLachlan, M. J.; Coombs, N.; Ozin, G. A. Periodic Mesoporous Organosilicas with Organic Groups inside the Channel Walls. *Nature* **1999**, *402*, 867–871.
(26) Manayil, J.; Lee, A.; Wilson, K. Functionalized Periodic Mesoporous Organosilicas: Tunable Hydrophobic Solid Acids for Biomass Conversion. *Molecules* **2019**, *24*, 239.
(27) Zhuravlev, L. T. The Surface Chemistry of Amorphous Silica. Zhuravlev Model. *Colloids Surf., A* **2000**, *173*, 1–38.
(28) Ek, S. Determination of the Hydroxyl Group Content in Silica by Thermogravimetry and a Comparison with ^{1}H MAS NMR Results. *Thermochim. Acta* **2001**, *379*, 201–212.
(29) Rice, G. L.; Scott, S. L. Characterization of Silica-Supported Vanadium(V) Complexes Derived from Molecular Precursors and Their Ligand Exchange Reactions. *Langmuir* **1997**, *13*, 1545–1551.
(30) Jelinek, L.; sz. Kovats, E. True Surface Areas from Nitrogen Adsorption Experiments. *Langmuir* **1994**, *10*, 4225–4231.
(31) Hammes, K.; Smernik, R. J.; Skjemstad, J. O.; Schmidt, M. W. I. Characterisation and Evaluation of Reference Materials for Black Carbon Analysis Using Elemental Composition, Colour, BET Surface Area and ^{13}C NMR Spectroscopy. *Appl. Geochem.* **2008**, *23*, 2113–2122.
(32) Catalan, J.; Perez, P.; Laynez, J.; Blanco, F. G. Analysis of the Solvent Effect on the Photophysics Properties of 6-Propionyl-2-(Dimethylamino)Naphthalene (PRODAN). *J. Fluoresc.* **1991**, *1*, 215–223.
(33) Reichardt, C.; Welton, T. *Solvents and Solvent Effects in Organic Chemistry*, 4th edn.; Wiley-VCH: Weinheim, 2011.
(34) Zhuravlev, L. T. Concentration of Hydroxyl Groups on the Surface of Amorphous Silicas. *Langmuir* **1987**, *3*, 316–318.
(35) Humbert, B. Estimation of Hydroxyl Density at the Surface of Pyrogenic Silicas by Complementary NMR and Raman Experiments. *J. Non-Cryst. Solids* **1995**, *191*, 29–37.
(36) Gallas, J.-P.; Goupil, J.-M.; Vimont, A.; Lavalley, J.-C.; Gil, B.; Gilson, J.-P.; Miserque, O. Quantification of Water and Silanol Species on Various Silicas by Coupling IR Spectroscopy and In-Situ Thermogravimetry. *Langmuir* **2009**, *25*, 5825–5834.
(37) Mrowiec-Bialoń, J. Determination of Hydroxyls Density in the Silica-Mesostructured Cellular Foams by Thermogravimetry. *Thermochim. Acta* **2006**, *443*, 49–52.
(38) Shioji, S.; Kawaguchi, M.; Hayashi, Y.; Tokami, K.; Yamamoto, H. Rehydroxylation of Dehydrated Silica Surfaces by Water Vapor Adsorption. *Adv. Powder Technol.* **2001**, *12*, 331–342.
(39) Ide, M.; El-Roz, M.; De Canck, E.; Vicente, A.; Planckaert, T.; Bogaerts, T.; Van Driessche, I.; Lynen, F.; Van Speybroeck, V.; Thybault-Starzyk, F.; Van Der Voort, P. Quantification of Silanol Sites for the Most Common Mesoporous Ordered Silicas and Organosilicas: Total versus Accessible Silanols. *Phys. Chem. Chem. Phys.* **2013**, *15*, 642–650.
(40) Xu, X.; Zhao, Y.; Wang, J.; Zhang, N.; Wang, C.; Zhang, J.; Wei, N. Water Flow inside Various Geometric Nano-Confinement Channels. *Phys. Chem. Chem. Phys.* **2020**, *22*, 24633–24639.
(41) Tohidi, M.; Toghraie, D. The Effect of Geometrical Parameters, Roughness and the Number of Nanoparticles on the Self-Diffusion Coefficient in Couette Flow in a Nanochannel by Using of Molecular Dynamics Simulation. *Physica B Condens. Matter.* **2017**, *518*, 20–32.

(42) Wei, M.-J.; Zhou, J.; Lu, X.; Zhu, Y.; Liu, W.; Lu, L.; Zhang, L. Diffusion of Water Molecules Confined in Slits of Rutile TiO_2(110) and Graphite(0001). *Fluid Phase Equilib.* **2011**, *302*, 316–320.
(43) Mietner, B. J.; Fröba, M.; Valiullin, R. Water Transport in Periodic Mesoporous Organosilica Materials. *J. Phys. Chem. C* **2018**, *122*, 12673–12680.
(44) Yoo, H.; Paranji, R.; Pollack, G. H. Impact of Hydrophilic Surfaces on Interfacial Water Dynamics Probed with NMR Spectroscopy. *J. Phys. Chem. Lett.* **2011**, *2*, 532–536.
(45) Bordallo, H. N.; Aldridge, L. P.; Churchman, G. J.; Gates, W. P.; Telling, M. T. F.; Kiefer, K.; Fouquet, P.; Seydel, T.; Kimber, S. A. J. Quasi-Elastic Neutron Scattering Studies on Clay Interlayer-Space Highlighting the Effect of the Cation in Confined Water Dynamics. *J. Phys. Chem. C* **2008**, *112*, 13982–13991.
(46) Fujita, S.; Inagaki, S. Self-Organization of Organosilica Solids with Molecular-Scale and Mesoscale Periodicities. *Chem. Mater.* **2008**, *20*, 891–908.
(47) Stock, P.; Monroe, J. I.; Utzig, T.; Smith, D. J.; Shell, M. S.; Valtiner, M. Unraveling Hydrophobic Interactions at the Molecular Scale Using Force Spectroscopy and Molecular Dynamics Simulations. *ACS Nano* **2017**, *11*, 2586–2597.
(48) Monroe, J. I.; Shell, M. S. Decoding Signatures of Structure, Bulk Thermodynamics, and Solvation in Three-Body Angle Distributions of Rigid Water Models. *J. Chem. Phys.* **2019**, *151*, 094501.
(49) Silva, C.; Martins, M.; Jing, S.; Fu, J.; Cavaco-Paulo, A. Practical Insights on Enzyme Stabilization. *Crit. Rev. Biotechnol.* **2018**, *38*, 335–350.
(50) Carey, C.; Cheng, Y.-K.; Rossky, P. J. Hydration Structure of the α-Chymotrypsin Substrate Binding Pocket: The Impact of Constrained Geometry. *Chem. Phys.* **2000**, *258*, 415–425.
(51) Bai, P.; Siepmann, J. I.; Deem, M. W. Adsorption of Glucose into Zeolite Beta from Aqueous Solution. *AIChE J.* **2013**, *59*, 3523–3529.
(52) Di Iorio, J. R.; Johnson, B. A.; Román-Leshkov, Y. Ordered Hydrogen-Bonded Alcohol Networks Confined in Lewis Acid Zeolites Accelerate Transfer Hydrogenation Turnover Rates. *J. Am. Chem. Soc.* **2020**, *142*, 19379–19392.
(53) Cordon, M. J.; Harris, J. W.; Vega-Vila, J. C.; Bates, J. S.; Kaur, S.; Gupta, M.; Witzke, M. E.; Wegener, E. C.; Miller, J. T.; Flaherty, D. W.; Hibbitts, D. D.; Gounder, R. Dominant Role of Entropy in Stabilizing Sugar Isomerization Transition States within Hydrophobic Zeolite Pores. *J. Am. Chem. Soc.* **2018**, *140*, 14244–14266.
(54) Serva, A.; Salanne, M.; Havenith, M.; Pezzotti, S. Size Dependence of Hydrophobic Hydration at Electrified Gold/Water Interfaces. *Proc. Natl. Acad. Sci. U. S. A.* **2021**, *118*, e2023867118.
(55) Mileo, P. G. M.; Rogge, S. M. J.; Houlleberghs, M.; Breynaert, E.; Martens, J. A.; Van Speybroeck, V. Interfacial Study of Clathrates Confined in Reversed Silica Pores. *J. Mater. Chem. A* **2021**, *9*, 21835–21844.
(56) Bai, D.; Chen, G.; Zhang, X.; Sum, A. K.; Wang, W. How Properties of Solid Surfaces Modulate the Nucleation of Gas Hydrate. *Sci. Rep.* **2015**, *5*, 12747.
(57) Cha, M.; Shin, K.; Lee, H.; Moudrakovski, I. L.; Ripmeester, J. A.; Seo, Y. Kinetics of Methane Hydrate Replacement with Carbon Dioxide and Nitrogen Gas Mixture Using in Situ NMR Spectroscopy. *Environ. Sci. Technol.* **2015**, *49*, 1964–1971.
(58) Mietner, J. B.; Brieler, F. J.; Lee, Y. J.; Fröba, M. Properties of Water Confined in Periodic Mesoporous Organosilicas: Nanoimprinting the Local Structure. *Angew. Chem. Int. Ed.* **2017**, *56*, 12348–12351.
(59) Conti Nibali, V.; Pezzotti, S.; Sebastiani, F.; Galimberti, D. R.; Schwaab, G.; Heyden, M.; Gaigeot, M.-P.; Havenith, M. Wrapping Up Hydrophobic Hydration: Locality Matters. *J. Phys. Chem. Lett.* **2020**, *11*, 4809–4816.
(60) Isaienko, O.; Nihonyanagi, S.; Sil, D.; Borguet, E. Observation of the Bending Mode of Interfacial Water at Silica Surfaces by Near-Infrared Vibrational Sum-Frequency Generation Spectroscopy of the [Stretch + Bend] Combination Bands. *J. Phys. Chem. Lett.* **2013**, *4*, 531–535.
(61) Chien, J. C. W. A Study of Surface Structures of Submicron Metal Oxides by Vanadium Tetrachloride as a Paramagnetic Probe. *J. Am. Chem. Soc.* **1971**, *93*, 4675–4684.
(62) Peri, J. B.; Hensley, A. L. The Surface Structure of Silica Gel. *J. Phys. Chem.* **1968**, *72*, 2926–2933.
(63) Cyran, J. D.; Donovan, M. A.; Vollmer, D.; Siro Brigiano, F.; Pezzotti, S.; Galimberti, D. R.; Gaigeot, M.-P.; Bonn, M.; Backus, E. H. G. Molecular Hydrophobicity at a Macroscopically Hydrophilic Surface. *Proc. Natl. Acad. Sci. U. S. A.* **2019**, *116*, 1520–1525.
(64) Zhang, J.; Tan, J.; Pei, R.; Ye, S.; Luo, Y. Ordered Water Layer on the Macroscopically Hydrophobic Fluorinated Polymer Surface and Its Ultrafast Vibrational Dynamics. *J. Am. Chem. Soc.* **2021**, *143*, 13074–13081.
(65) Rajamani, S.; Truskett, T. M.; Garde, S. Hydrophobic Hydration from Small to Large Lengthscales: Understanding and Manipulating the Crossover. *Proc. Natl. Acad. Sci. U. S. A.* **2005**, *102*, 9475–9480.
(66) Huang, D. M.; Chandler, D. The Hydrophobic Effect and the Influence of Solute−Solvent Attractions. *J. Phys. Chem. B* **2002**, *106*, 2047–2053.
(67) Wu, X.; Lu, W.; Streacker, L. M.; Ashbaugh, H. S.; Ben-Amotz, D. Temperature-Dependent Hydrophobic Crossover Length Scale and Water Tetrahedral Order. *J. Phys. Chem. Lett.* **2018**, *9*, 1012–1017.
(68) Grdadolnik, J.; Merzel, F.; Avbelj, F. Origin of Hydrophobicity and Enhanced Water Hydrogen Bond Strength near Purely Hydrophobic Solutes. *Proc. Natl. Acad. Sci. U.S.A.* **2017**, *114*, 322–327.
(69) Xiao, S.; Myers, M.; Miao, Q.; Sanaur, S.; Pang, K.; Steigerwald, M. L.; Nuckolls, C. Molecular Wires from Contorted Aromatic Compounds. *Angew. Chem., Int. Ed.* **2005**, *44*, 7390–7394.
(70) Tacke, R.; Mallak, M.; Willeke, R. Pentacoordination of Silicon by Four Covalent Si−S Bonds and One Covalent Si−C Bond. *Angew. Chem., Int. Ed.* **2001**, *113*, 2401–2403.
(71) Beagley, B.; Monaghan, J. J.; Hewitt, T. G. Electron-Diffraction Studies of Tetramethylsilane and Hexamethyldisilane, and Discussion of the Lengths of Si-C Bonds. *J. Mol. Struct.* **1971**, *8*, 401–411.
(72) Huang, D. M.; Chandler, D. Temperature and Length Scale Dependence of Hydrophobic Effects and Their Possible Implications for Protein Folding. *Proc. Natl. Acad. Sci. U. S. A.* **2000**, *97*, 8324–8327.
(73) Perera, P. N.; Fega, K. R.; Lawrence, C.; Sundstrom, E. J.; Tomlinson-Phillips, J.; Ben-Amotz, D. Observation of Water Dangling OH Bonds around Dissolved Nonpolar Groups. *Proc. Natl. Acad. Sci. U. S. A.*. **2009**, *106*, 12230–12234.
(74) Jani, A.; Busch, M.; Mietner, J. B.; Ollivier, J.; Appel, M.; Frick, B.; Zanotti, J.-M.; Ghoufi, A.; Huber, P.; Fröba, M.; Morineau, D. Dynamics of Water Confined in Mesopores with Variable Surface Interaction. *J. Chem. Phys.* **2021**, *154*, 094505.
(75) Esquivel, D.; Ouwehand, J.; Meledina, M.; Turner, S.; Tendeloo, G. V.; Romero-Salguero, F. J.; Clercq, J. D.; Voort, P. V. D. Thiol-Ethylene Bridged PMO: A High Capacity Regenerable Mercury Adsorbent via Intrapore Mercury Thiolate Crystal Formation. *J. Hazard. Mater.* **2017**, *339*, 368–377.
(76) Sanchez, C.; Jeremias, F.; Ernst, S.-J.; Henninger, S. K. Synthesis, Functionalization and Evaluation of Ethylene-Bridged PMOs as Adsorbents for Sorption Dehumidification and Cooling Systems. *Micropor. Mesopor. Mat.* **2017**, *244*, 151–157.
(77) Yang, Q.; Liu, J.; Yang, J.; Kapoor, M. P.; Inagaki, S.; Li, C. Synthesis, Characterization, and Catalytic Activity of Sulfonic Acid-Functionalized Periodic Mesoporous Organosilicas. *J. Catal.* **2004**, *228*, 265–272.
(78) Armstrong, B. D.; Han, S. Overhauser Dynamic Nuclear Polarization to Study Local Water Dynamics. *J. Am. Chem. Soc.* **2009**, *131*, 4641–4647.
(79) Franck, J. M.; Kausik, R.; Han, S. Overhauser Dynamic Nuclear Polarization-Enhanced NMR Relaxometry. *Micropor. Mesopor. Mat.* **2013**, *178*, 113–118.
(80) Armstrong, B. D.; Han, S. A New Model for Overhauser Enhanced Nuclear Magnetic Resonance Using Nitroxide Radicals. *J. Chem. Phys.* **2007**, *127*, 104508.
(81) Abraham, M. J.; Murtola, T.; Schulz, R.; Páll, S.; Smith, J. C.; Hess, B.; Lindahl, E. GROMACS: High Performance Molecular Simulations through Multi-Level Parallelism from Laptops to Supercomputers. *SoftwareX* **2015**, *1–2*, 19–25.
(82) Horn, H. W.; Swope, W. C.; Pitera, J. W.; Madura, J. D.; Dick, T. J.; Hura, G. L.; Head-Gordon, T. Development of an Improved Four-

Site Water Model for Biomolecular Simulations: TIP4P-Ew. *J. Chem. Phys.* **2004**, *120*, 9665–9678.
(83) Emami, F. S.; Puddu, V.; Berry, R. J.; Varshney, V.; Patwardhan, S. V.; Perry, C. C.; Heinz, H. Force Field and a Surface Model Database for Silica to Simulate Interfacial Properties in Atomic Resolution. *Chem. Mater.* **2014**, *26*, 2647–2658.
(84) Swails, J.; Hernandez, C.; Mobley, D. L.; Nguyen, H.; Wang, L. P.; Janowski, P. ParmEd: Cross-Program Parameter and Topology File Editor and Molecular Mechanical Simulator Engine Http://Parmed.Github.Io/ParmEd/Html/Index.Html (Accessed Dec 5, 2016).
(85) Malde, A. K.; Zuo, L.; Breeze, M.; Stroet, M.; Poger, D.; Nair, P. C.; Oostenbrink, C.; Mark, A. E. An Automated Force Field Topology Builder (ATB) and Repository: Version 1.0. *J. Chem. Theory Comput.* **2011**, *7*, 4026–4037.
(86) Stroet, M.; Caron, B.; Visscher, K. M.; Geerke, D. P.; Malde, A. K.; Mark, A. E. Automated Topology Builder Version 3.0: Prediction of Solvation Free Enthalpies in Water and Hexane. *J. Chem. Theory Comput.* **2018**, *14*, 5834–5845.
(87) Berendsen, H. J. C.; Postma, J. P. M.; van Gunsteren, W. F.; DiNola, A.; Haak, J. R. Molecular Dynamics with Coupling to an External Bath. *J. Chem. Phys.* **1984**, *81*, 3684–3690.
(88) Hoover, W. G. Canonical Dynamics: Equilibrium Phase-Space Distributions. *Phys. Rev. A* **1985**, *31*, 1695–1697.
(89) Martyna, G. J.; Klein, M. L.; Tuckerman, M. Nosé–Hoover Chains: The Canonical Ensemble via Continuous Dynamics. *J. Chem. Phys.* **1992**, *97*, 2635–2643.
(90) Swope, W. C.; Andersen, H. C.; Berens, P. H.; Wilson, K. R. A Computer Simulation Method for the Calculation of Equilibrium Constants for the Formation of Physical Clusters of Molecules: Application to Small Water Clusters. *J. Chem. Phys.* **1982**, *76*, 637–649.
(91) Hess, B.; Bekker, H.; Berendsen, H. J. C. LINCS: A Linear Constraint Solver for Molecular Simulations. *J. Comput. Chem.* **1997**, *18*, 10.
(92) Essmann, U.; Perera, L.; Berkowitz, M. L.; Darden, T.; Lee, H.; Pedersen, L. G. A Smooth Particle Mesh Ewald Method. *J. Chem. Phys.* **1995**, *103*, 8577–8593.
(93) Nguyen, H.; Roe, D. R.; Swails, J.; Case, D. A. PYTRAJ: Interactive Data Analysis for Molecular Dynamics Simulations (Accessed Dec 5, 2016).

Table of Contents artwork